NeuroImage 245 (2021) 118699

Contents lists available at ScienceDirect

NeuroImage

journal homepage: www.elsevier.com/locate/neuroimage

Individual differences in error-related frontal midline theta activity during visuomotor adaptation

Zeb D. Jonker[a,b,d,*], Rick van der Vliet[a,b], Guido Maquelin[a], Joris van der Cruijsen[b], Gerard M. Ribbers[b,d], Ruud W. Selles[b,c], Opher Donchin[e], Maarten A. Frens[a]

[a] Department of Neuroscience, Erasmus MC, University Medical Center Rotterdam, Rotterdam, 3015 CN, The Netherlands
[b] Department of Rehabilitation Medicine, Erasmus MC, University Medical Center Rotterdam, Rotterdam, 3015 CN, The Netherlands
[c] Department of Plastic and Reconstructive Surgery, Erasmus MC, University Medical Center Rotterdam, Rotterdam, 3015 CN, The Netherlands
[d] Rijndam Rehabilitation, 3015LJ Rotterdam, The Netherlands
[e] Department of Biomedical Engineering and Zlotowski Center for Neuroscience, Ben Gurion University of the Negev, 8499000, Be'er Sheva, Israel

A B S T R A C T

Post-feedback frontal midline EEG activity has been found to correlate with error magnitude during motor adaptation. However, the role of this neuronal activity remains to be elucidated. It has been hypothesized that post-feedback frontal midline activity may represent a prediction error, which in turn may be directly related to the adaptation process or to an unspecific orienting response. To address these hypotheses, we replicated a previous visuomotor adaptation experiment with very small perturbations, likely to invoke implicit adaptation, in a new group of 60 participants and combined it with EEG recordings. We found error-related peaks in the frontal midline electrodes in the time domain. However, these were best understood as modulations of frontal midline theta activity (FMT, 4–8 Hz). Trial-level differences in FMT correlated with error magnitude. This correlation was robust even for very small errors as well as in the absence of imposed perturbations, indicating that FMT does not depend on explicit or strategic re-aiming. Within participants, trial-level differences in FMT were not related to between-trial error corrections. Between participants, individual differences in FMT-error-sensitivity did not predict differences in adaptation rate. Taken together, these results imply that FMT does not drive implicit motor adaptation. Finally, individual differences in FMT-error-sensitivity negatively correlate to motor execution noise. This suggests that FMT reflects saliency: larger execution noise means a larger standard deviation of errors so that a fixed error magnitude is less salient. In conclusion, this study suggests that frontal midline theta activity represents a saliency signal and does not directly drive motor adaptation.

1. Introduction

In motor learning, movement errors are used to update motor commands for subsequent actions. We call this process motor adaptation. Motor adaptation can occur within a trial during continuous movements, or between trials during discrete ballistic movements such as swinging a golf club or throwing darts. In motor adaptation tasks, perturbations of visual or proprioceptive feedback drive adjustments of the motor command to achieve the intended goal of the movement. These adjustments may reflect unconscious implicit adaptation, conscious explicit strategy, or both (Taylor et al., 2014). Typically, smaller gradual perturbations result in implicit adaptation whereas larger sudden perturbations have been found to induce explicit strategy (Malfait and Ostry, 2004; Morehead et al., 2015; Werner et al., 2019).

Linear dynamical models of error-based learning that include an adaptation rate, a retention rate, planning noise (state noise), and execution noise (output noise) have been shown to qualitatively resemble between-trial implicit adaptation of reaching movements to a gradual perturbation signal with incremental perturbation steps (Cheng and Sabes, 2007). In this model class, planning noise represents stochastic noise in central movement planning, whereas execution noise represents stochastic noise in peripheral movement execution that is not included in the motor command (van Beers, 2009). Van der Vliet et al. (2018) showed that such a model can also explain differences in motor learning between individuals. In that study we presented a novel Bayesian fitting procedure to estimate the model parameters for each individual participant. In agreement with optimal Kalman filter theory (Kalman, 1960; Wei and Körding, 2010), individuals with relatively more planning noise and less execution noise showed a higher adaptation rate than individuals with relatively less planning noise and more execution noise. However, an important question regarding these mathematical models is the extent to which they reflect the reality of the underlying neurophysiological processes (Tan et al., 2016).

Independently from the mathematical modeling approach, electroencephalography (EEG) has been used increasingly to explore neurophysiological correlates of learning. Most studies have focused on frontal midline activity, which has been found to correlate with error magnitude in motor adaptation tasks (Anguera et al., 2009; Arrighi et al., 2016; Aziz et al., 2020; Krigolson et al., 2008; Maclean et al., 2015; Reuter et al., 2018; Torrecillos et al., 2014; Vocat et al., 2011). However, a recent study with very small gradual perturbations did not

* Corresponding Author at: Department of Neuroscience, Erasmus MC, PO Box 2040, 3000 CA, Rotterdam, The Netherlands.
E-mail address: z.jonker@erasmusmc.nl (Z.D. Jonker).

https://doi.org/10.1016/j.neuroimage.2021.118699.
Received 28 July 2021; Received in revised form 26 September 2021; Accepted 30 October 2021
Available online 14 November 2021.

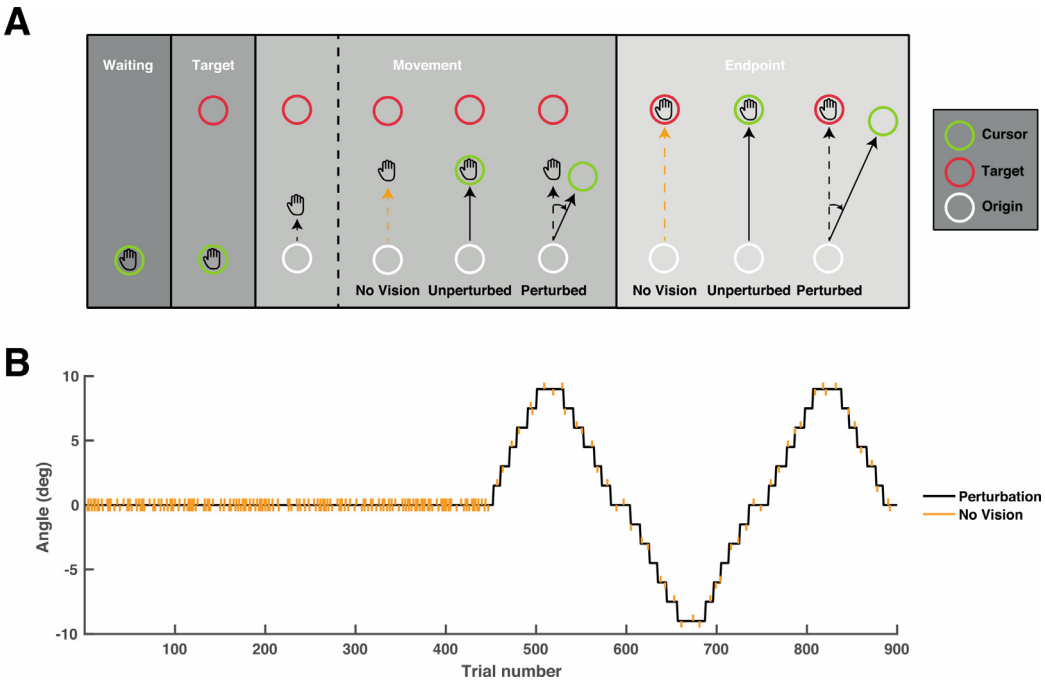

Fig. 1. Design of the experiment. **A:** Trial design. **B:** Experimental design.

find a relation between error magnitude and frontal midline activity (Palidis et al., 2019). Error-related activity in the frontal midline region is often expressed as an amplitude in the time domain, or as modulations of theta activity (4–8 Hz) in the frequency domain (Arrighi et al., 2016; Cavanagh et al., 2012). Torrecillos et al. (2014) found that frontal midline activity associated with angular errors closely resembled the topography and timing of feedback-related negativity (Miltner et al., 1997). Due to this resemblance, the authors hypothesized that frontal midline error activity may represent a prediction error, which they suggest may be related to the motor adaptation process or to an unspecific orienting response. However, to our knowledge, no prior studies have tested these hypotheses.

To address these hypotheses, we conjoined a mathematical model approach and an electroencephalography approach. We replicated our previous visuomotor adaptation experiment (van der Vliet et al., 2018) in a new group of 60 participants and combined it with EEG recordings. The current study explores (1) whether error-related frontal midline activity will be evoked in the absence of perturbations; (2) whether frontal midline activity is related to between-trial error corrections; (3) whether individual differences in error-related frontal midline activity are related to individual differences in motor learning.

Regarding the third objective, our previous experiment (van der Vliet et al., 2018) showed that adaptation rate was positively correlated to planning noise and negatively correlated to execution noise. Furthermore, the standard deviation of the signed errors (angular distance from the target) was negatively related to adaptation rate and positively related to planning noise and execution noise. The current study explores how individual differences in error-related frontal midline activity fit within this behavioral framework.

2. Material and methods

2.1. Participants

We recruited 60 right-handed (Oldfield, 1971) participants (19 men and 41 women; mean age = 25.6 years, range = 18–61) without any medical condition that might interfere with motor performance. Participants received a small financial token for traveling and time compensation. The study was performed in accordance with the Declaration of Helsinki and was approved by the medical ethics committee of the Erasmus MC University Medical centre.

2.2. Experimental procedure

The experimental procedure was adapted from van der Vliet et al. (2018). Participants were seated in front of a horizontal projection screen with a robotic handle underneath. This handle was situated at elbow height and could be moved in the horizontal plane. The position of the handle was projected on top of the screen as a cursor (green circle 5 mm diameter). Furthermore, the screen displayed an origin (white circle 10 mm diameter) and a target (red circle 10 mm diameter) at fixed positions. The origin was located approximately 40 cm straight in front of the participant and the target was projected exactly 10 cm behind the origin, approximately 50 cm in front of the participant. Participants were instructed to hold the handle in their dominant right hand and move the cursor from the origin through the target in one smooth ballistic reaching movement. To prevent direct feedback of hand position underneath the screen, participants were wearing an apron that was secured to the top of the screen.

The experiment consisted of three types of trials: no-vision, unperturbed, and perturbed trials (Fig. 1A). At the start of each trial, participants held the cursor in the origin. The target appeared after one second, indicating that the participant should start the movement. In all trial types, the cursor disappeared when the handle left the origin. In no-vision trials, the cursor did not reappear during the entire movement. In unperturbed and perturbed trials, the cursor reappeared when the handle distance from the origin exceeded 5 cm. However, in perturbed trials, the cursor was projected at a predefined angle relative to the actual handle position.

The movement was damped with a force cushion (3.6Ns/m, ramped up over 7.5 ms) when the handle position exceeded 10 cm distance from the origin, and thus exceeded the target distance. We defined this time point as movement offset. In perturbed and unperturbed trials, the cursor froze at this time point to provide feedback on the endpoint error. Furthermore, the target changed color. If the movement duration was too short (< 400 ms), the target stayed red; if the movement duration

was correct (400–600 ms), the target turned white; and if the duration was too long (> 600 ms), the target turned blue. We instructed participants that these colors were merely a guideline to ensure ballistic movements without online adjustments and emphasized that the goal of the task was to hit the target. One second after onset of the force cushion, the robot pushed the handle back to the starting position. When the handle was at the origin, the cursor reappeared at the handle position.

The experiment consisted of 900 trials, divided into two blocks of 450 trials: a baseline block followed by a perturbation block (Fig. 1B). The exact order of the trial types was randomized for each participant. The baseline block contained 225 unperturbed trials and 225 no-vision trials in a completely randomized order. In contrast, the perturbation block contained 400 perturbation trials and 50 no-vision trials in a pseudorandomized order: in every epoch of 9 trials, there was one randomly interspersed no-vision trial. Thus, the experiment contained 625 trials with visual feedback. In the perturbation block, the perturbation angle changed from 0° to 9° to −9° and back to 0° with increments of 1.5° every 8 to 12 trials. The experiment was paused after every 150 trials for approximately 2 min.

2.3. Movement recording and preprocessing

The experiment was controlled by a custom C++ program. The position and velocity signals of the robot handle were sampled at 500 Hz. The velocity signal was filtered with an exponential moving average filter (smoothing factor = 0.18 s). Movement onset was defined as the time point when movement velocity exceeded 0.03 m/s and movement offset was defined as the moment that the hand location exceeded 10 cm distance from the starting position. The hand angle was defined as the angle between the vector connecting the origin and the hand at the end of the movement, relative to the vector connecting the origin and the target. The clockwise direction was defined as positive. Trials were removed if movement duration exceeded 1 s or if the absolute hand angle exceeded 30°. On average, 1% (range [0 18]) of the total 900 movement trials were excluded per participant.

2.4. Movement analysis

From the movement recordings, we estimated the execution noise, planning noise, and adaptation rate of each participant. The analysis was performed with Bayesian Markov Chain Monte Carlo simulations in JAGS version 4.3.0 (available from: https://sourceforge.net/projects/mcmc-jags/) and is extensively described in van der Vliet et al. (2018). In short, we fitted a state-space model of trial-to-trial behavior (Cheng and Sabes, 2006) to the movement data of all participants.

$$x[s,n+1] = A[s] * x[s,n] - B[s] * e[s,n] + \eta[s,n] \quad (1)$$

$$y[s,n] = x[s,n] + \varepsilon[s,n] \quad (2)$$

$$e[s,n] = y[s,n] + p[s,n] \quad (3)$$

$$\eta[s,n] \sim N\left(0, \sigma_\eta^2[s]\right) \quad (4)$$

$$\varepsilon[s,n] \sim N\left(0, \sigma_\varepsilon^2[s]\right) \quad (5)$$

For each trial n of participant s, $x[s,n]$ is the movement plan, $y[s,n]$ the angle of the hand relative to the target at the endpoint, $p[s,n]$ the perturbation angle and $e[s,n]$ the error angle of the cursor on the screen relative to the target (signed error). Participant-specific motor adaptation parameters estimated with this model are the retention rate $A[s]$, which is the fractional retention of the movement plan $x[s,n]$ in the previous trial, and the adaptation rate $B[s]$, which is the fractional change caused by the error $e[s,n]$ in the previous trial. The noise terms include planning noise $\eta[s,n]$, and execution noise $\varepsilon[s,n]$. Planning noise and execution noise are modeled as zero-mean Gaussians. The standard deviations of these Gaussians $\sigma_\eta[s]$ and $\sigma_\varepsilon[s]$ represent the magnitude of planning and execution noise for each participant. The participant-specific motor learning parameters were estimated hierarchically with uninformative priors. Additionally, we calculated the standard deviation of the signed errors (σ_y) for each participant to explore possible indirect effects between the participant-specific motor learning parameters and error-related frontal midline activity. Since trials 301–450 and 751–900 were used to estimate error-related frontal midline theta activity in the baseline block and the perturbation block (see EEG analysis below), we performed the movement analysis without these trials.

2.5. EEG recording and preprocessing

Participants were wearing a 128 channel EEG cap connected to a 136 channel REFA system (TMSi, Oldenzaal, The Netherlands). The EEG data were recorded with a sampling rate of 2048 Hz from 62 EEG channels: FP1, FPz, FP2, AF7, AF3, AF4, AF8, F7, F5, F3, F1, Fz, F2, F4, F6, F8, FT7 FC5, FC3, FC1, FCz, FC2, FC4, FC6, FT8, T7, C5, C3, C1, Cz, C2, C4, C6, T8, TP7, CP5, CP3, CP1, CPz, CP2, CP4, CP6, TP8, P7, P5, P3, P1, Pz, P2, P4, P6, P8, PO7, PO5, PO3, POz, PO4, PO6, PO8, O1, Oz, O2, and 2 EOG channels. The EOG electrodes were located between the eyebrows and to the right of the right eye. Impedance was kept below 4 kΩ. The recording of each channel was referenced to the average signal across all channels.

After recording, the EEG signals were preprocessed with the EEGLAB toolbox (version 14.1.2b; Swartz Center for Computational Neuroscience, La Jolla, USA) and custom scripts in MATLAB version 2018b (Mathworks, Natick, USA). The raw average referenced EEG signals were digitally filtered between 2–40 Hz with a 6th order Butterworth filter, cut into trial epochs of 2000 ms centered around the onset of visual feedback, and down-sampled to 128 Hz. Non-stereotypical artifacts were automatically removed by excluding trials in which the average log power was an outlier compared to the other trials within the same channel (absolute z-score >3.5). Data quality of the remaining trials was verified by visual inspection. Similarly, stereotypical artifacts were automatically removed by performing a fast-independent component analysis (Delorme et al., 2007) and excluding components in which the average log power was an outlier (absolute z-score >3.5). Visual inspection confirmed that the removed components corresponded to eye movements. The other components were projected back to the channel space. On average, 40 (range [14 79]) of the 900 EEG traces were excluded and 1.1 (range [1 2]) of the 64 components were removed. The remaining traces were used for analysis in the time domain.

For the analysis in the frequency domain, the remaining EEG traces were first filtered with a surface Laplacian to improve the spatial resolution (Perrin et al., 1989). Subsequently, the traces were decomposed into their time-frequency representations using Morlet wavelet convolution applied to the concatenated trial data (Cohen, 2014; Tallon-Baudry et al., 1996). The wavelet frequencies ranged from 2 to 30 Hz in 29 steps of 1 Hz (with the number of cycles ranging from 4 to 10 in 29 logarithmically-spaced steps, respectively, for the 29 frequencies). After convolution, the deconcatenated traces were trimmed between –800 ms and 800 ms, and centered on the onset of visual feedback to remove edge artifacts. Consecutively, the log power at each time-frequency point within each trial was normalized as a percentage change relative to the average log power of that frequency in the predefined baseline window (from 800 ms until 600 ms before visual feedback) across all trials for the subject.

2.6. EEG analysis

The EEG analysis was performed separately for the baseline block and the perturbation block. We used linear mixed-effects models (MATLAB's fitlme function) to estimate trial-level effects across participants.

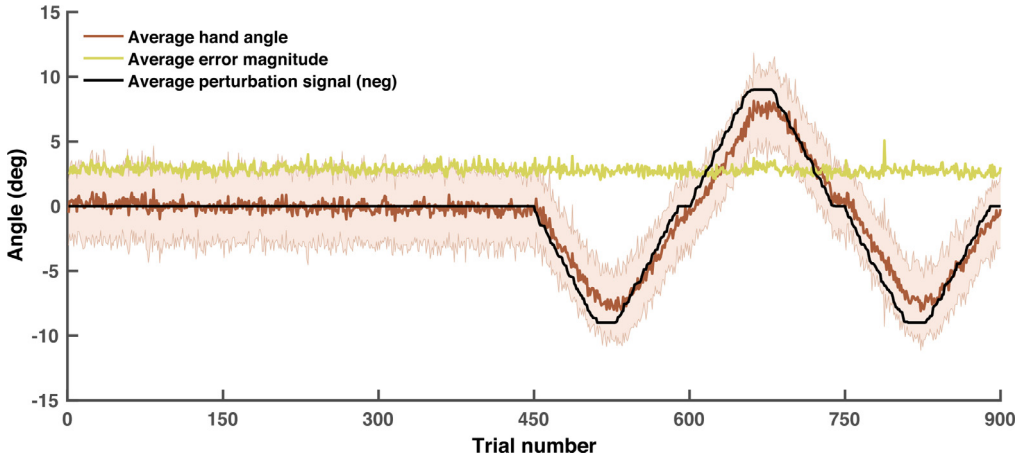

Fig. 2. Average movement data across participants throughout the experiment. The error bars on the brown line indicate the standard deviation of the hand angle across subjects.

All variables were z-score normalized for the purpose of the regression. Tables show the normalized effects in order to compare their relative strength. When effect sizes are shown in their original units, they have been transformed back using the standard deviations of the dependent and independent variables. Error magnitude was defined as the absolute angle between the cursor on the screen relative to the target, and error correction was defined as the absolute change in the hand angle in the subsequent trial (Tan et al., 2016). In the EEG analysis, we only included trials with visual feedback.

For the trial-level analysis in the frequency domain, a separate regression was used for each time-frequency window. We used a large window (4–8 Hz and 100–600 ms) to analyze frontal midline theta activity (FMT) in channel FCz (Arrighi et al., 2016; Cavanagh et al., 2012; Savoie et al., 2018) and fine-grained time-frequency windows to generate figures. For a given time-frequency window, we regressed average EEG power on error magnitude, movement correction, and feedback color (which indicated whether movement duration was within the desired range, see above).

$$EEG[s,n] \sim \alpha[s] + \beta_1[s] * |e|[s,n] + \beta_2[s] * |c|[s,n] + \beta_3[s] * f[s,n] \quad (6)$$

For each trial n of participant s, $EEG[s,n]$ is the average EEG power in a time-frequency window, $|e|[s,n]$ is the error magnitude, $|c|[s,n]$ is the movement correction in the subsequent trial, and $f[s,n]$ is a categorical variable indicating if the movement duration was "too short", "too long" or "appropriate". All participant-specific estimates were modeled as random effects around the group average fixed effects.

We used training sets to select the variables and test sets to estimate their effect size. The training and test sets were trials 1–300 and 301–450 for the baseline block, and trials 451–750 and 751–900 for the perturbation block. In the training sets, we compared different versions of the model with the Akaike Information Criterion (AIC) and the Mean Squared Error (MSE) after 10-fold cross-validation stratified over participants. In the test sets, we used the selected model to estimate the effect size of the parameters. FMT-error-sensitivity was defined as the relation between frontal midline theta power (FMT) and error magnitude ($\beta_1[s]$). In other time-frequency windows, we refer to the coefficient of the error magnitude ($\beta_1[s]$) as the EEG-error-sensitivity.

2.7. Participant-level analysis

In the participant level analysis, we tested for linear relationships between FMT-error-sensitivity ($\beta 1[s]$), planning noise $\sigma_\eta[s]$, execution noise $\sigma_\varepsilon[s]$, and adaptation rate $B[s]$. We used multivariate linear regressions (MATLAB's fitlm function) to test two regression models specifically: FMT-error-sensitivity regressed on the noises and adaptation rate, and adaptation rate regressed on the noises and the FMT-error-sensitivity. The choice of these two models reflects an underlying assumption that the noises characterize the individual.

$$B[s] \sim \alpha + \gamma_1 * \sigma_\eta[s] + \gamma_2 * \sigma_\varepsilon[s] + \gamma_3 * \beta_1[s] \quad (7)$$

$$\beta_1[s] \sim \alpha + \gamma_1 * \sigma_\eta[s] + \gamma_2 * \sigma_\varepsilon[s] + \gamma_3 * B[s] \quad (8)$$

In these models, we used the participant-specific point estimates from the movement analysis and the trial-level EEG analysis. For the participant-level analysis, FMT-error-sensitivity was estimated on the pooled test sets (trials 301–450 and trials 751–900 combined). To prevent double use of trials, the motor learning parameters were estimated on the other trials. In order to compare the strength of the correlations, all variables were z-score normalized. We compared different versions of the model with the Akaike Information Criterion (AIC) and the Mean Squared Error (MSE) after leave-one-out cross-validation

3. Results

3.1. Results of movement analysis

On average, target onset, movement onset, and movement offset occurred at −441 ms (range across participants [-512 -401]), -193 ms [−247 −151] and 78 ms [50 118] respectively, relative to the onset of visual feedback. Over the course of the experiment, participants adapted their reaching movements to the perturbation signal (Fig. 2). As a result, the average error magnitude was similar in the baseline block and the perturbation block (Fig. 2). In 38% [23 49] of the trials, the cursor was completely inside the target (error magnitude < 1.43°) and in an additional 46% [39 51] of the trials, the cursor was partially inside the target (error magnitude < 4.29°). The Bayesian fitting procedure showed that the average planning noise, execution noise, and adaptation rate were 0.48° [0.22 0.79], 2.47° [1.40 4.36], and 0.14 [0.08 0.23], respectively.

3.2. Results of EEG analysis

In channel FCz, the trials without visual feedback showed a large peak between 100 and 600 milliseconds after visual feedback (Fig. 3A,B). Trials with visual feedback showed a wave-like pattern superimposed on that peak (Fig. 3A,B). The amplitude of this wave scaled with error magnitude (Fig. 3C,D) and the frequency of this wave corresponded to power in the theta band (Fig. 3E,F). The signal in the frequency domain contains less noise and is unipolar, which makes the analysis less susceptible for the borders of the timewindow. Throughout the experiment overall theta power in the 100–600 ms time window declined, but the relation between theta power and error magnitude

Table 1
Trial-level analysis in the baseline training set (trial 1–300). Linear mixed-effects model with frontal midline theta power (FMT) as the dependent variable (Eq. (6)). In order to compare the effect sizes, all variables were z-score normalized. The last row shows the full model in which α represents the intercept and β_1, β_2, β_3, represent the relationship with error magnitude, error correction, and movement duration (β_{3a} is too short and β_{3b} is too long). In addition to the effect size estimations, different versions of the model were compared with the Akaike Information Criterion (AIC) and the Mean Squared Error (MSE) after 10-fold cross-validation stratified over participants. Trial-level differences in FMT in the baseline block were best explained by error magnitude (model 2).

	FMT baseline block	a estimate (95% CI) *p-value*	β_1 estimate (95% CI) *p-value*	β_2 estimate (95% CI) *p-value*	β_{3a} estimate (95% CI) *p-value*	β_{3b} estimate (95% CI) *p-value*	AIC	MSE
1.	a	.00 (−.08 0.08) *.997*	–	–	–	–	23,498	.92
2.	$a + \beta_1$	**.01 (−.07 0.09) *.729***	**.19 (0.15 0.23) *<0.001***	**–**	**–**	**–**	**23,222**	**.89**
3.	$a + \beta_2$	.00 (−.07 0.08) *.925*	–	.09 (0.07 0.12) *<0.001*	–	–	23,431	.91
4.	$a + \beta_3$	.00 (−.08 0.08) *.999*	–	–	.04 (−.08 0.16) *.514*	-0.01 (−.09 0.07) *.801*	23,507	.92
5.	$a + \beta_1 + \beta_2$	.01 (−.07 0.09) *.729*	.18 (0.14 0.23) *<0.001*	.00 (−.02 0.03) *.807*	–	–	23,226	.89
6.	$a + \beta_1 + \beta_3$	.02 (−.06 0.10) *.698*	.19 (0.15 0.23) *<0.001*	–	.01 (−.10 0.13) *.835*	-0.02 (−.10 0.07) *.726*	23,230	.89
7.	$a + \beta_2 + \beta_3$	.01 (−.07 0.08) *.898*	–	.09 (0.07 0.12) *<0.001*	.03 (−.09 0.14) *.660*	−0.02 (−.10 0.06) *.671*	23,440	.91
8.	$a + \beta_1 + \beta_2 + \beta_3$	.02 (−.06 0.10) *.698*	.19 (0.14 0.23) *<0.001*	.00 (−.02 0.03) *.805*	.01 (−.10 0.13) *.837*	-0.02 (−.10 0.07) *.722*	23,234	.89

Table 2
Trial-level analysis in the perturbation training set (trial 451–750). Linear mixed-effects model with frontal midline theta power (FMT) as the dependent variable (Eq. (6)). In order to compare the effect sizes, all variables were z-score normalized. The last row shows the full model in which α represents the intercept and β_1, β_2 and β_3, represent the relationship with error magnitude, error correction, and movement duration (β_{3a} is too short and β_{3b} is too long). In addition to the effect size estimations, different versions of the model were compared with the Akaike Information Criterion (AIC) and the Mean Squared Error (MSE) after 10-fold cross-validation stratified over participants. Trial-level differences in FMT in the perturbation block were best explained by error magnitude (model 2).

	FMT perturbation block	a estimate (95% CI) *p-value*	β_1 estimate (95% CI) *p-value*	β_2 estimate (95% CI) *p-value*	β_{3a} estimate (95% CI) *p-value*	β_{3b} estimate (95% CI) *p-value*	AIC	MSE
1.	α	.00 (−.07 0.06) *.940*	–	–	–	–	41,547	.94
2.	$a + \beta_1$	**.01 (−.06 0.08) *.798***	**.17 (0.13 0.21) *<0.001***	**–**	**–**	**–**	**41,060**	**.91**
3.	$a + \beta_2$	.00 (−.06 0.07) *.953*	–	.07 (0.05 0.10) *<0.001*	–	–	41,465	.93
4.	$a + \beta_3$	.00 (−.06 0.06) *.883*	–	–	.04 (−.05 0.14) *.335*	.01 (−.05 0.08) *.687*	41,549	.94
5.	$a + \beta_1 + \beta_2$	.01 (−.06 0.08) *.772*	.17 (0.13 0.21) *<0.001*	.01 (−.02 0.03) *.554*	–	–	41,058	.91
6.	$a + \beta_1 + \beta_3$	.01 (−.06 0.08) *.836*	.17 (0.13 0.21) *<0.001*	–	.03 (−.06 0.12) *.474*	.01 (−.05 0.07) *.760*	41,064	.91
7.	$a + \beta_2 + \beta_3$	.00 (−.07 0.07) *.996*	–	.07 (0.05 0.10) *<0.001*	.04 (−.05 0.14) *.341*	.01 (−.06 0.07) *.822*	41,468	.93
8.	$a + \beta_1 + \beta_2 + \beta_3$	.01 (−.06 0.08) *.810*	.17 (0.13 0.21) *<0.001*	.01 (−.02 0.03) *.567*	.03 (−.06 0.12) *.457*	.01 (−.05 0.07) *.760*	41,063	.91

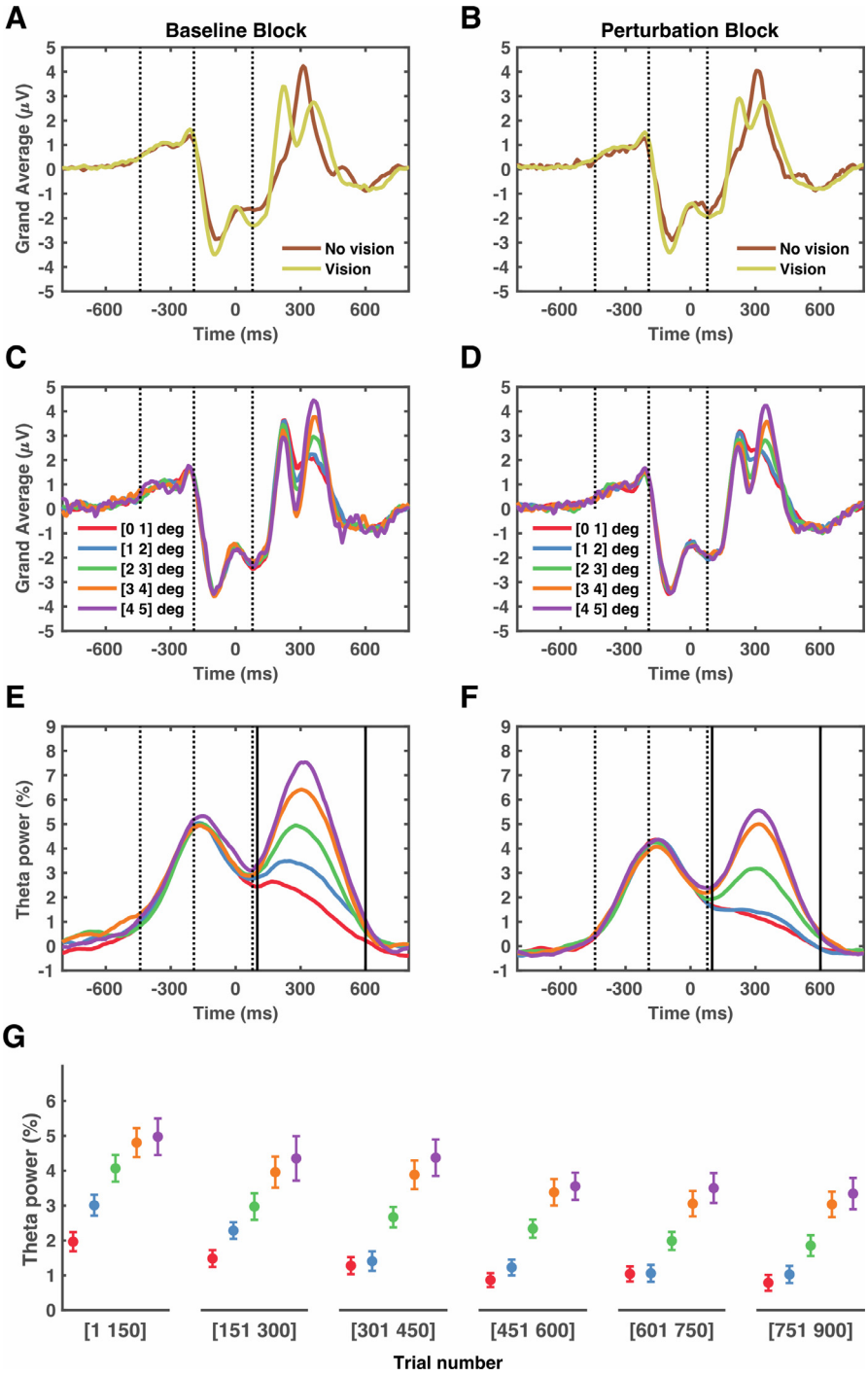

Fig. 3. Average EEG data in channel FCz across participants. For visualization purposes, trials have been binned and averaged based on error magnitude. Black dotted lines represent the average target onset (−441 ms), movement onset (−193 ms) and movement end (78 ms), relative to the onset of visual feedback. Black solid lines represent the post-feedback window (100–600 ms). **A,B:** Average EEG amplitude across subjects in the vision versus the no-vision trials. **C,D:** Average EEG amplitude across subjects. **E,F:** Average theta power (4–8 Hz) across subjects. **G:** Average theta power in the post-feedback window throughout the experiment. Trials 1–450 are part of the baseline block and thus without any perturbations. Error bars represent the standard error of the mean.

(FMT-error-sensitivity) was consistent throughout the baseline and perturbation blocks (Fig. 3G).

Consistent with what is shown in Fig. 3, trial-level differences in FMT in the baseline and perturbation training sets were best explained by error magnitude (Tables 1,2). Any apparent relation between FMT and error correction in the subsequent trial disappeared when error magnitude was included in the model. Furthermore, feedback color did not further explain trial-level differences in FMT. Thus, we used the linear mixed model without error correction and feedback color to estimate FMT-error-sensitivity, expressed as the change in average frontal midline theta power per degree of error magnitude. The average FMT-error sensitivity was 0.61%/degree (range across participants [0.02 1.61] in the baseline test set and 0.56%/degree [−0.24 1.67] in the perturbation test set. For the participant-level analysis below, we pooled the trials of both test sets to estimate FMT-error-sensitivity (0.57%/degree [−0.13 1.77]).

Fig. 4 illustrates that our definition of FMT appropriately captured the EEG signal of interest. Figs. 4A and B illustrate that EEG-error-sensitivity in channel FCz was most prominent in the theta (4–8 Hz) frequency band, with foothills in the delta (2–3 Hz) and alpha (9–14 Hz) frequency bands. Furthermore, Fig. 4C and D illustrate that EEG-error-sensitivity in the theta band was most prominent in channels FCz and Cz.

3.3. Results of participant-level analysis

The point estimates from the movement analysis and the EEG analysis were used to explore the relation between individual differences

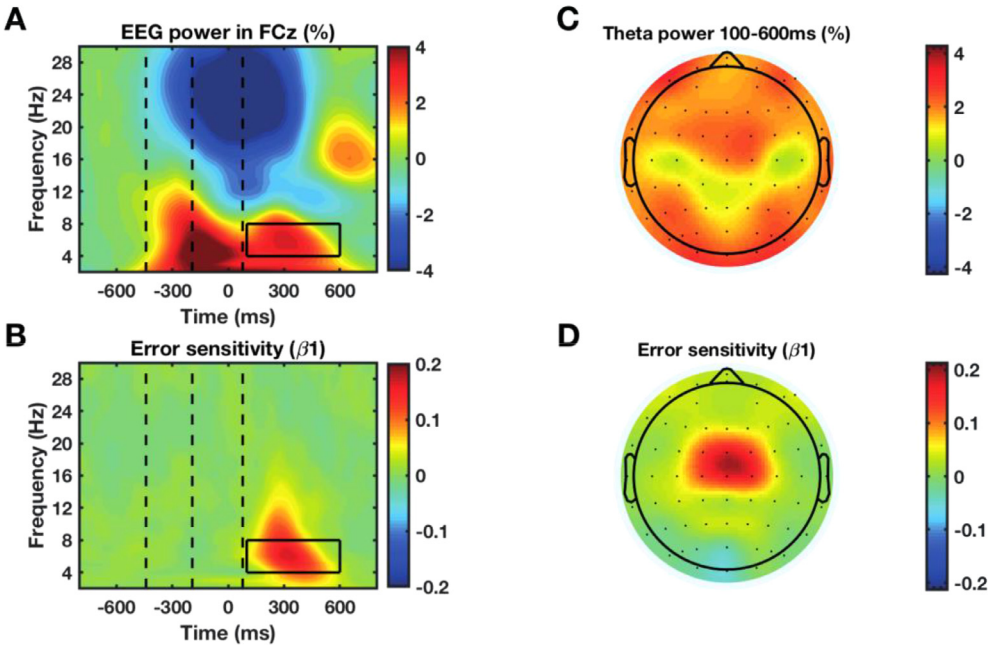

Fig. 4. Error sensitivity in other time-frequency windows (**A,B**) and other channels (**C,D**). **A:** EEG power in FCz. Dotted lines represent the average target onset (−441 ms), movement onset (−193 ms) and movement end (78 ms), relative to the onset of visual feedback. Solid lines represent the time-frequency window (100–600 ms and 4–8 Hz) used in the EEG analysis. **B:** Relation between EEG power and error magnitude. **C:** Average post-feedback theta power (4–8 Hz) in other channels. **D:** Relation between theta power and error magnitude.

in the motor learning parameters and individual differences in FMT-error sensitivity (Tables 3,4). Individual differences in adaptation rate were positively correlated to planning noise (Fig. 5A) and negatively related to execution noise (Fig. 5B), and were not further explained by FMT-error-sensitivity (Fig. 5C). Conversely, individual differences in FMT-error-sensitivity were best explained by execution noise (Fig. 5E), and not further explained by planning noise (Fig. 5D), nor adaptation rate (Fig. 5F). These results mirror the relative contribution of the motor learning parameters to individual differences in standard deviation of signed errors (σ_y). In this experimental design, execution noise had a much larger contribution to the standard deviation of signed errors (Fig. 5G) compared to planning noise (Fig. 5H) and adaptation rate (Fig. 5I). Supplementary Fig. 1 shows that the results of the participant-level analysis were comparable when we used all 900 trials for the movement analysis and all 625 trials with visual feedback for the EEG analysis, rather than separate subsets.

Fig. 6 shows the data of the individuals with the lowest, median and highest execution noise. This figure illustrates that higher execution noise was related to lower adaptation rate (Fig. 6A–C) and lower FMT-error-sensitivity (Fig. 6D–F).

4. Discussion

This study shows that post-feedback frontal midline theta activity (FMT) is related to error magnitude, even in the absence of evoked perturbations. Furthermore, this study shows that FMT is not related to between-trial error corrections. Finally, this study shows that the sensitivity of FMT to error magnitude is smaller for participants with greater execution noise. With 60 participants and 625 trials with visual feedback per participant, this is the largest study on visuomotor adaptation and EEG activity to date, allowing us to investigate individual differences in motor learning and FMT. In group average EEG activity, FMT appeared to reflect error magnitude (Fig. 3). However, this relationship between FMT and error magnitude (FMT-error-sensitivity) was much weaker in individuals with a larger execution noise (Fig. 5E) and thus a larger standard deviation of signed errors (Fig. 5H). As further explained below, our results suggest that frontal midline theta activity represents a saliency signal, that does not directly drive implicit motor adaptation.

First, this study shows that frontal midline theta activity (FMT) is related to error magnitude, even in the absence of imposed perturbations. This is in apparent contrast with existing literature. Arrighi et al. (2016) only found a relationship between frontal midline activity and error magnitude for error magnitudes above a certain threshold. Palidis et al. (2019) only used very small gradual perturbations and did not see a relationship between frontal midline activity and error magnitude. Savoie et al. (2018) found that FMT, corrected for error magnitude, was higher when participants were made aware of the perturbation paradigm and instructed how to counteract it. These previous studies imply that the relation between frontal midline activity and error magnitude depends on awareness of the perturbation paradigm. However, the current study shows that FMT-error-sensitivity is related to error magnitude during very small perturbations and even in the absence of imposed perturbations (during the baseline block). Under such conditions, it is safe to assume that adaptation was implicit. This indicates that FMT does not depend on awareness of the perturbation paradigm.

Second, this study shows that trial-level differences in FMT are not related to between-trial error corrections. To our knowledge, this is the first study to investigate the relation between EEG activity and adaptation on the trial level. Our results are a strong argument that frontal midline activity does not amplify implicit motor adaptation, which is thought to be dependent on the olivocerebellar system (De Zeeuw et al., 2011; Shadmehr and Krakauer, 2008). Since FMT is related to the absolute error rather than the signed error, it cannot be used as the main error signal for motor adaptation. Nonetheless, FMT could be used as an auxiliary error signal that weights the importance of the main error signal and thus drives adaptation (Kim et al., 2019; Torrecillos et al., 2014). However, the current study shows no relation between trial-level differences in FMT and between-trial error corrections, indicating that FMT does not directly drive implicit motor adaptation.

Finally, this study shows that individual differences in FMT-error sensitivity are negatively correlated to individual differences in execution noise. This supports the hypothesis of Torrecillos et al. (2014) that FMT during motor adaptation reflects saliency. For participants with a larger execution noise and thus a larger standard deviation of signed errors, the same absolute error is less surprising. An alternative suggestion is that frontal midline activity represents reward prediction error (Palidis et al., 2019). Reward prediction error and saliency are difficult to distinguish (Cavanagh and Frank, 2014; Sambrook and Goslin, 2015). However, the scalar relation between FMT and error magnitude beyond binary target 'hits' and 'straddles' (Kim et al., 2019) is more compatible with the saliency hypothesis.

Table 3
Participant-level analysis with adaptation rate (B) as the dependent variable (Eq. (7)). In order to compare the effect sizes, all variables were z-score normalized. The last row shows the full model in which α represents the intercept and γ_1, γ_2 and γ_3 represent the relationship with planning noise (σ_η), execution noise (σ_ε), FMT-error-sensitivity (β_1). In addition to the effect size estimations, different versions of the model were compared with the Akaike Information Criterion (AIC) and the Mean Squared Error (MSE) after leave-one-out cross-validation. Individual differences in adaptation rate were best explained by planning noise and execution noise (model 5).

	Adaptation rate	a estimate (95% CI) *p-value*	γ_1 estimate (95% CI) *p-value*	γ_2 estimate (95% CI) *p-value*	γ_3 estimate (95% CI) *p-value*	AIC	MSE
1.	α	0 (−.26 0.26) *1.000*	–	–	–	173	1.02
2.	$a+\gamma_1$	0 (−.26 0.26) *1.000*	.08 (−.18 0.35) *.523*	–	–	173	1.04
3.	$a+\gamma_2$	0 (−.23 0.23) *1.000*	–	-0.44 (−.67 −.20) *<0.001*	–	161	.85
4.	$a+\gamma_3$	0 (−.25 0.25) *1.000*	–	–	*.29* *(0.04 0.54)* *.026*	168	.97
5.	$a+\gamma_1+\gamma_2$	**0** **(−.22 0.22)** ***1.000***	***.34*** ***(0.09 0.59)*** ***.009***	***-0.58*** ***(−.83 −.33)*** ***<0.001***	**–**	**155**	**.78**
6.	$a+\gamma_1+\gamma_3$	0 (−.25 0.25) *1.000*	.16 (−.09 0.42) *.210*	–	.33 (0.07 0.59) *.014*	168	.97
7.	$a+\gamma_2+\gamma_3$	0 (−.23 0.23) 1.000	–	-0.38 (−.64 −.13) *.004*	.13 (−.12 0.39) *.301*	161	.86
8.	$a+\gamma_1+\gamma_2+\gamma_3$	0 (−.22 0.22) *1.000*	.35 (0.10 0.60) *.006*	-0.52 (−.79 −.26) *<0.001*	.16 (−.08 0.41) *.186*	155	.78

Table 4
Participant-level analysis with FMT-error-sensitivity (β_1) as the dependent variable (Eq. (8)). In order to compare the effect sizes, all variables were z-score normalized. The last row shows the full model in which α represents the intercept and γ_1, γ_2 and γ_3 represent the relationship with planning noise (σ_η), execution noise (σ_ε), and adaptation rate (B). In addition to the effect size estimations, different versions of the model were compared with the Akaike Information Criterion (AIC) and the Mean Squared Error (MSE) after leave-one-out cross-validation. Individual differences in FMT-error-sensitivity were best explained by execution noise (model 3).

	FMT-error-sensitivity	a estimate (95% CI) *p-value*	γ_1 estimate (95% CI) *p-value*	γ_2 estimate (95% CI) *p-value*	γ_3 estimate (95% CI) *p-value*	AIC	MSE
1.	α	0 (−.26 0.26) *1.000*	–	–	–	173	1.02
2.	$a+\gamma_1$	0 (−.25 0.25) *1.000*	-0.24 (−.50 0.01) *.061*	–	–	170	.99
3.	$a+\gamma_2$	**0** **(−.24 0.24)** ***1.000***	**–**	**-0.40** **(−.64 −.16)** ***.002***	**–**	**163**	**.88**
4.	$a+\gamma_3$	0 (−.25 0.25) *1.000*	–	–	*.29* *(0.04 0.54)* *.026*	168	.97
5.	$a+\gamma_1+\gamma_2$	0 (−.24 0.24) *1.000*	-0.09 (−.35 0.18) *.527*	-0.36 (−.63 −.09) *.009*	–	164	.91
6.	$a+\gamma_1+\gamma_3$	0 (−.24 0.24) *1.000*	-0.27 (−.51 −.02) *.032*	–	.31 (0.07 0.55) *.014*	165	.92
7.	$a+\gamma_2+\gamma_3$	0 (−.24 0.24) *1.000*	–	-0.34 (−.61 −.07) *.014*	*.14* *(−.13 0.41)* *.301*	164	.90
8.	$a+\gamma_1+\gamma_2+\gamma_3$	0 (−.24 0.24) *1.000*	-0.15 (−.43 0.13) *.295*	-0.25 (−.57 0.06) *.116*	.19 (−.09 0.47) *.186*	165	.91

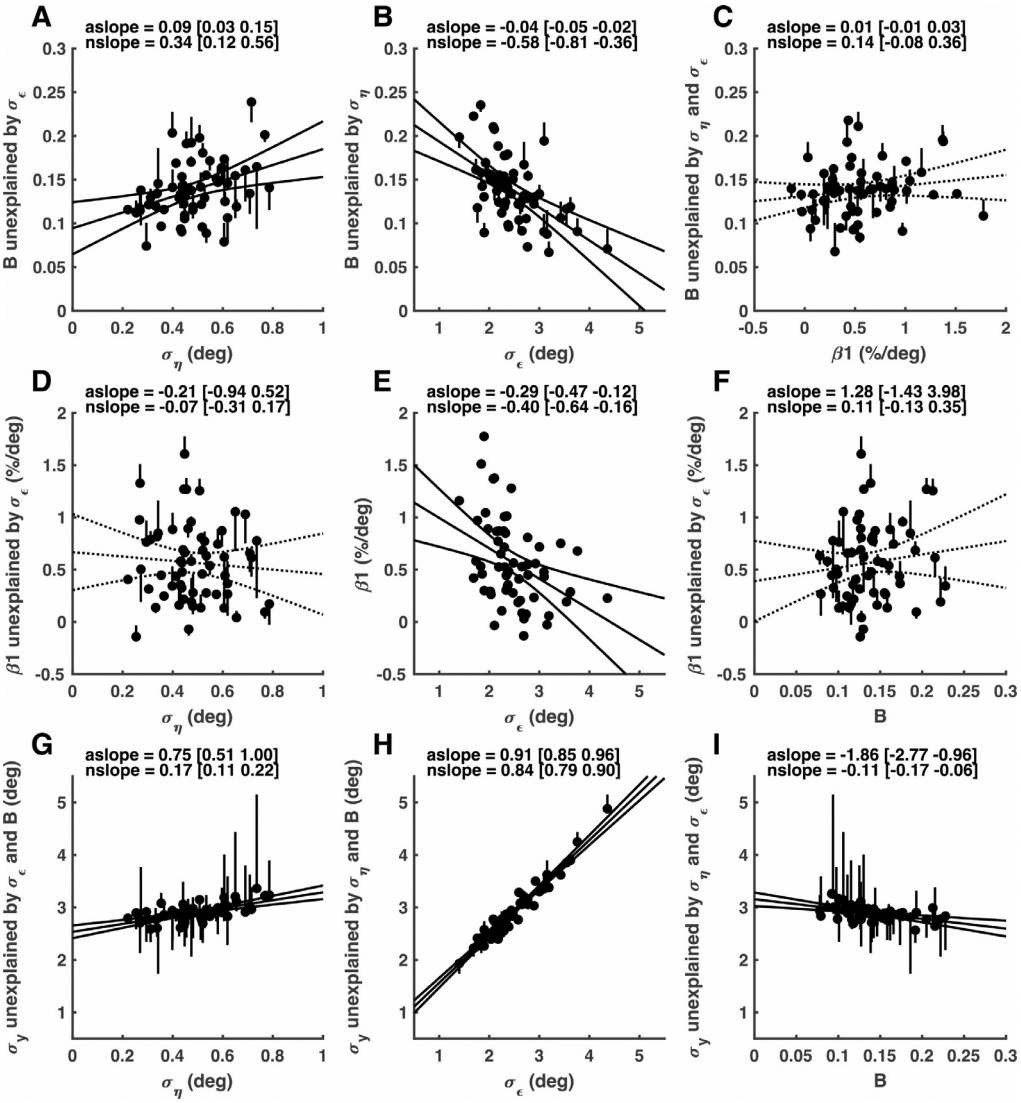

Fig. 5. Participant-level analysis (60 participants). The vertical lines represent the dependent variable. The dots at the end of the lines represent the residuals of the dependent variable after subtracting the estimated effect of the (other) independent variables included in the best model. Black lines represent the absolute slope ('aslope') and the confidence interval. The z-score normalized slope is also shown ('nslope'). **A–C:** Linear model with adaptation rate (B) as the dependent variable (Eq. (7)). The best model included planning noise (σ_η) and execution noise (σ_ϵ), but not FMT-error-sensitivity (β_1) (Table 3, Model 5). Note that the confidence intervals of z-score normalized slope ('nslope') of planning noise (σ_η) and execution noise (σ_ϵ) are slightly smaller than in Table 3, because, in this figure, the effect of the other parameter is 'fixed' in order to create the residuals. **D,F:** Linear model with FMT-error-sensitivity (β_1) as the dependent variable (Eq. (8)). The best model included execution noise (σ_ϵ), but not planning noise (σ_η) nor adaptation rate (B) (Table 4, Model 3). **G–I:** Linear model with the standard deviation of signed errors (σ_y), as the dependent variable. In the full model with planning noise (σ_η), execution noise (σ_ϵ) and adaptation rate (B), execution noise was the dominant factor.

Individual differences in FMT-error sensitivity were not related to adaptation rate when properly controlled for execution noise. Conversely, individual differences in adaptation rate were positively related to planning noise, negatively related to execution noise and were not further explained by FMT-error-sensitivity. These results on the participant level support our interpretation that FMT does not drive implicit adaptation. Furthermore, the current study replicates our earlier findings (van der Vliet et al., 2018), which strengthens the evidence that the adaptation rate is tuned to the noise terms according to Kalman filter theory (Kalman, 1960; Wei and Körding, 2010). Fig. 7 illustrates the relation between individual differences in planning noise, execution noise, and adaptation rate. Supplementary Fig. 2 illustrates how individual differences in FMT-error-sensitivity fit within this behavioral framework.

This study is limited by the focus on implicit motor adaptation on the trial level and the participant level. We did not expose our participants to different experimental conditions. The perturbation steps were so small that the average absolute error was similar in the baseline and the perturbation block. This is also reflected in our movement analysis, which assumes that planning noise and adaptation rate are constant throughout the experiment. Moreover, we did not purposely introduce noise and reward in the experiment. Therefore, we cannot generalize our results to experiments with larger perturbation steps or otherwise more salient errors that may induce explicit strategy. Furthermore, we should be cautious when generalizing our results to experiments with changing conditions. However, within our focus we can conclude that FMT reflects saliency and does not drive implicit motor adaptation.

In conclusion, this visuomotor adaptation experiment indicates that the modulation of post-movement frontal midline theta activity (FMT) reflects a prediction error that does not drive implicit adaptation. In decision-making tasks, it has been suggested that FMT drives cognitive control (Cavanagh and Frank, 2014). We hypothesize that the same is true in motor adaptation. While our study does show that FMT is not de-

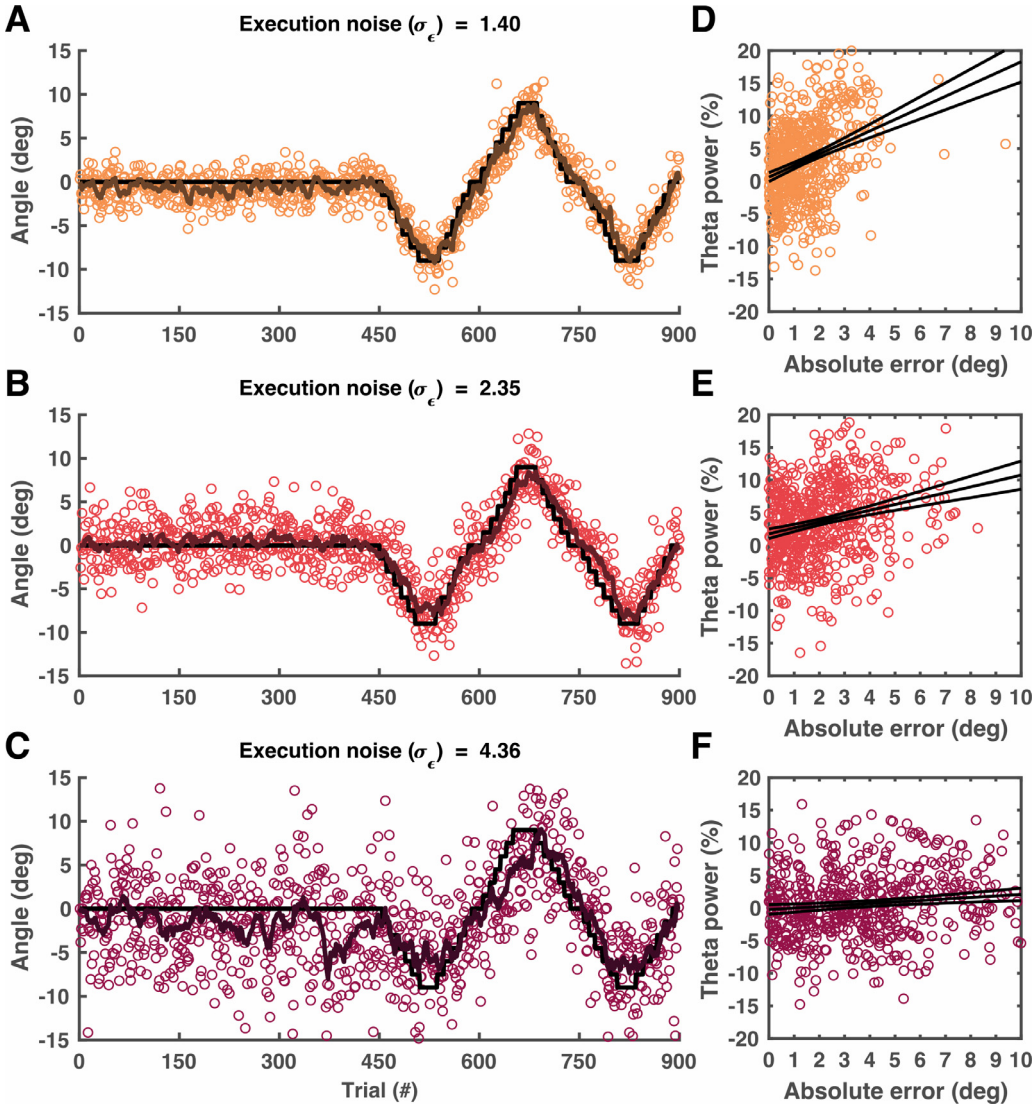

Fig. 6. Data of three individuals with increasing execution noise (σ_ϵ). **A–C:** Movement data. Colored circles represent the hand angle in individual trials. The colored lines represent the estimated movement plan from the Bayesian fitting procedure. **D–F:** EEG data. Colored circles represent the post-feedback theta power in individual trials. Black lines represent the slope (FMT-error-sensitivity) and its confidence interval.

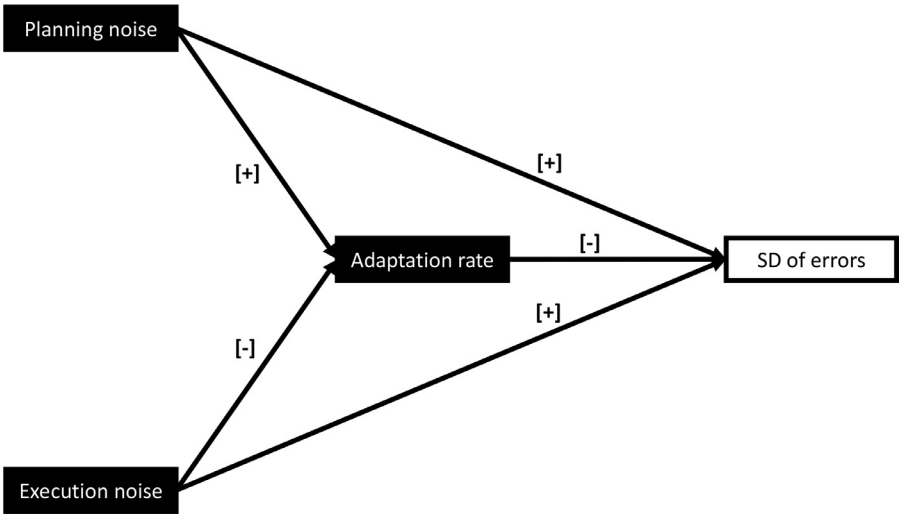

Fig. 7. Schematic representation of the relationship between individual differences in planning noise, execution noise, and adaptation rate. Individuals with relatively more planning noise and less execution noise showed a higher adaptation rate than individuals with relatively less planning noise and more execution noise. Furthermore, individuals with more motor noise (planning noise and execution noise) showed a larger standard deviation of signed errors (SD of errors), whereas individuals with a higher adaptation rate showed a lower standard deviation of errors. These results indicate that planning noise directly increases the standard deviation of errors but indirectly decreases the standard deviation of errors through its effect on adaptation rate, whereas execution noise both directly and indirectly increases the standard deviation of errors.

pendent on awareness, FMT may nevertheless influence awareness and cognitive control. This, in turn, might evoke cognitive strategies such as cautious movement, memorization, and re-aiming. In individuals with larger execution noise, errors must be proportionally greater to indicate a change in the external environment that warrants activation of cognitive control. Another plausible alternative is that FMT tunes planning noise to different environmental conditions. This would induce search behavior in conditions with high estimation uncertainty (Dhawale et al., 2019; Tan et al., 2016). Thus, an experiment where estimation uncertainty and explicit strategies are manipulated independently may clarify how FMT response ultimately affects behavior.

Data and code availability statement

The data that support the findings of this study are available from the corresponding author, ZJ, upon reasonable request.

Declaration of Competing Interest

None.

Credit authorship contribution statement

Zeb D. Jonker: Conceptualization, Methodology, Software, Formal analysis, Writing – original draft, Writing – review & editing. **Rick van der Vliet:** Methodology, Software, Writing – review & editing. **Guido Maquelin:** Methodology, Investigation, Writing – review & editing. **Joris van der Cruijsen:** Software, Writing – review & editing. **Gerard M. Ribbers:** Supervision, Writing – review & editing. **Ruud W. Selles:** Supervision, Writing – review & editing. **Opher Donchin:** Methodology, Supervision, Writing – review & editing. **Maarten A. Frens:** Methodology, Supervision, Writing – review & editing.

Acknowledgments

We would like to thank Nicole Malfait and Dimitrios J. Palidis for constructive feedback on the manuscript.

Supplementary materials

Supplementary material associated with this article can be found, in the online version, at doi:10.1016/j.neuroimage.2021.118699.

References

Anguera, J.A., Seidler, R.D., Gehring, W.J., 2009. Changes in performance monitoring during sensorimotor adaptation. J. Neurophysiol. 102, 1868–1879. doi:10.1152/jn.00063.2009.

Arrighi, P., Bonfiglio, L., Minichilli, F., Cantore, N., Carboncini, M.C., Piccotti, E., Rossi, B., Andre, P., 2016. EEG theta dynamics within frontal and parietal cortices for error processing during reaching movements in a prism adaptation study altering visuomotor predictive planning. PLoS ONE 11, 1–27. doi:10.1371/journal.pone.0150265.

Aziz, J.R., MacLean, S.J., Krigolson, O.E., Eskes, G.A., 2020. Visual feedback modulates aftereffects and electrophysiological markers of prism adaptation. Front. Hum. Neurosci. 14, 1–15. doi:10.3389/fnhum.2020.00138.

Cavanagh, J.F., Frank, M.J., 2014. Frontal theta as a mechanism for cognitive control. Trends Cogn. Sci. 18, 414–421. doi:10.1016/j.tics.2014.04.012.

Cavanagh, J.F., Zambrano-Vazquez, L., Allen, J.J.B., 2012. Theta lingua franca: a common mid-frontal substrate for action monitoring processes. Psychophysiology 49, 220–238. doi:10.1111/j.1469-8986.2011.01293.x.

Cheng, S., Sabes, P.N., 2007. Calibration of visually guided reaching is driven by error-corrective learning and internal dynamics. J. Neurophysiol. 97, 3057–3069. doi:10.1152/jn.00897.2006.

Cheng, S., Sabes, P.N., 2006. Modeling sensorimotor learning with linear dynamical systems. Neural Comput 18, 760–793. doi:10.1162/neco.2006.18.4.760.

Cohen, M.X., 2014. Analyzing Neural Time Series Data: Theory and Practice. MIT Press.

De Zeeuw, C.I., Hoebeek, F.E., Bosman, L.W.J., Schonewille, M., Witter, L., Koekkoek, S.K., 2011. Spatiotemporal firing patterns in the cerebellum. Nat. Rev. Neurosci. 12, 327–344. doi:10.1038/nrn3011.

Delorme, A., Sejnowski, T., Makeig, S., 2007. Enhanced detection of artifacts in EEG data using higher-order statistics and independent component analysis. Neuroimage 34, 1443–1449. doi:10.1016/j.neuroimage.2006.11.004.

Dhawale, A.K., Miyamoto, Y.R., Smith, M.A., Ölveczky, B.P., 2019. Adaptive regulation of motor variability. Curr. Biol. 29, 3551–3562. doi:10.1016/j.cub.2019.08.052, e7.

Kalman, R.E., 1960. A new approach to linear filtering and prediction problems. J. Fluids Eng. Trans. ASME 82, 35–45. doi:10.1115/1.3662552.

Kim, H.E., Parvin, D.E., Ivry, R.B., 2019. The influence of task outcome on implicit motor learning. Elife 8, 1–28. doi:10.7554/eLife.39882.

Krigolson, O.E., Holroyd, C.B., Van Gyn, G., Heath, M., 2008. Electroencephalographic correlates of target and outcome errors. Exp. Brain Res. 190, 401–411. doi:10.1007/s00221-008-1482-x.

Maclean, S.J., Hassall, C.D., Ishigami, Y., Krigolson, O.E., Eskes, G.A., 2015. Using brain potentials to understand prism adaptation: the error-related negativity and the p300. Front. Hum. Neurosci. 9, 1–14. doi:10.3389/fnhum.2015.00335.

Malfait, N., Ostry, D.J., 2004. Is interlimb transfer of force-field adaptation a cognitive response to the sudden introduction of load? J. Neurosci. 24, 8084–8089. doi:10.1523/JNEUROSCI.1742-04.2004.

Miltner, W.H.R., Braun, C.H., Coles, M.G.H., 1997. Event-related brain potentials following incorrect feedback in a time-estimation task: evidence for a "generic" neural system for error detection. J. Cogn. Neurosci. 9, 788–798. doi:10.1162/jocn.1997.9.6.788.

Morehead, J.R., Qasim, S.E., Crossley, M.J., Ivry, R., 2015. Savings upon re-aiming in visuomotor adaptation. J. Neurosci. 35, 14386–14396. doi:10.1523/JNEUROSCI.1046-15.2015.

Oldfield, R.C., 1971. The assessment and analysis of handedness: the Edinburgh inventory. Neuropsychologia 9, 97–113. doi:10.1016/0028-3932(71)90067-4.

Palidis, D.J., Cashaback, J.G.A., Gribble, P.L., 2019. Neural signatures of reward and sensory error feedback processing in motor learning. J. Neurophysiol. 121, 1561–1574. doi:10.1152/jn.00792.2018.

Perrin, F., Pernier, J., Bertrand, O., … Echallier, J.F., 1989. Spherical splines for scalp potential and current density mapping. Electroencephalogr. Clin. Neurophysiol. 72, 184–187. doi:10.1016/0013-4694(89)90180-6.

Reuter, E.M., Pearcey, G.E.P., Carroll, T.J., 2018. Greater neural responses to trajectory errors are associated with superior force field adaptation in older adults. Exp. Gerontol. 110, 105–117. doi:10.1016/j.exger.2018.05.020.

Sambrook, T.D., Goslin, J., 2015. A Neural reward prediction error revealed by a meta-analysis of ERPs using great grand averages. Psychol. Bull. 141, 213–235. doi:10.1037/bul0000006.

Savoie, F.A., Thénault, F., Whittingstall, K., Bernier, .P..-M., 2018. Visuomotor prediction errors modulate EEG activity over parietal cortex. Sci. Rep. 8, 1–16. doi:10.1038/s41598-018-30609-0.

Shadmehr, R., Krakauer, J.W., 2008. A computational neuroanatomy for motor control. Exp. Brain Res. 185, 359–381. doi:10.1007/s00221-008-1280-5.

Tallon-Baudry, C., Bertrand, O., Delpuech, C., Pernier, J., 1996. Stimulus specificity of phase-locked and non-phase-locked 40 Hz visual responses in human. J. Neurosci. 16, 4240–4249. doi:10.1523/JNEUROSCI.16-13-04240.1996.

Tan, H., Wade, C., Brown, P., 2016. Post-movement beta activity in sensorimotor cortex indexes confidence in the estimations from internal models. J. Neurosci. 36, 1516–1528. doi:10.1523/JNEUROSCI.3204-15.2016.

Taylor, J.A., Krakauer, J.W., Ivry, R.B., 2014. Explicit and implicit contributions to learning in a sensorimotor adaptation task. J. Neurosci. 34, 3023–3032. doi:10.1523/JNEUROSCI.3619-13.2014.

Torrecillos, F., Albouy, P., Brochier, T., Malfait, N., 2014. Does the processing of sensory and reward-prediction errors involve common neural resources? Evidence from a frontocentral negative potential modulated by movement execution errors. J. Neurosci. 34, 4845–4856. doi:10.1523/JNEUROSCI.4390-13.2014.

van Beers, R.J., 2009. Motor learning is optimally tuned to the properties of motor noise. Neuron 63, 406–417. doi:10.1016/j.neuron.2009.06.025.

van der Vliet, R., Frens, M.a, Vreede, L.De, Jonker, Z., Ribbers, G.M., Selles, R.W., Geest, J.Van Der, Donchin, O., 2018. Individual differences in motor noise and adaptation rate are optimally related. eNeuro 5, 1–14. doi:10.1523/ENEURO.0170-18.2018.

Vocat, R., Pourtois, G., Vuilleumier, P., 2011. Parametric modulation of error-related ERP components by the magnitude of visuo-motor mismatch. Neuropsychologia 49, 360–367. doi:10.1016/j.neuropsychologia.2010.12.027.

Wei, K., Körding, K., 2010. Uncertainty of feedback and state estimation determines the speed of motor adaptation. Front. Comput. Neurosci. 4, 1–9. doi:10.3389/fncom.2010.00011.

Werner, S., Strüder, H.K., Donchin, O., 2019. Intermanual transfer of visuomotor adaptation is related to awareness. PLoS ONE 14, e0220748. doi:10.1371/journal.pone.0220748.